Iranian Polymer Journal
https://doi.org/10.1007/s13726-019-00695-6

ORIGINAL RESEARCH

A novel investigation on micro-phase separation of thermoplastic polyurethanes: simulation, theoretical, and experimental approaches

Iman Sahebi Jouibari[1] · Vahid Haddadi-Asl[1] · Mohammad Masoud Mirhosseini[1]

Received: 9 December 2018 / Accepted: 25 February 2019

Abstract

Thermoplastic polyurethanes (TPUs) based on soft segments with varying molecular weight and molecular architecture show interesting micro-phase separation, thermal, morphological, molecular dynamics, and rheological properties. In the present study, TPUs based on two types of polyols, i.e., poly(tetramethylene ether) (1000 and 2000 g/mol) and polycaprolactone (500 and 2000 g/mol), were synthesized. This work has aimed to combine synthetic procedures, physical–chemistry calculations, and molecular dynamics simulation to study the effect of structure and molecular weight of the soft segments on TPU properties. Extent and kinetics of micro-phase separation were quantified with several methods such as spectroscopy, time-sweep rheological analysis, product of interaction parameter and degree of polymerization (χN), thermal analysis, compressible regular solution model, molecular dynamics, and microscopy. The results showed that high molecular weight polyether- and low molecular weight polyester-based synthesized TPUs have the highest and the lowest micro-phase separations, respectively. Moreover, in each class of polyol, the degree of micro-phase separation was concurrently increased with soft-segment block length. However, competition between enthalpic and entropic factors in the study of the polyols led to different results by various methods. Moreover, from the mechanical properties viewpoint, ester-based TPUs showed higher Young's modulus and lower elongation-at-break compared to ether-based counterparts.

Keywords Polyurethane · Micro-phase separation · Block polymers · Interaction parameter · Molecular dynamics simulation

Introduction

Thermoplastic polyurethanes (TPUs), as one of the most important families of block polymers, are synthesized in various structures based on selection of different ingredients [1]. These AB-type block polymers are composed of hard segments (HS), formed by reaction of an isocyanate with a chain extender, and soft segments (SS), commonly formed by polyester or polyether macrodiols [2]. Micro-phase separation occurs due to the thermodynamic incompatibility of the soft and hard segments at low temperatures [3]. Degree of the micro-phase separation and morphology of the micro-phase-separated domains play a key role on the engineering properties of TPUs [4]. A large number of factors such as polymerization procedure, chemical structure of ingredients, segmental length, crystallization ability of hard and soft segments, hard/soft-segment ratio, and process parameters which affect the morphology and micro-phase separation of TPUs [5].

Effect of soft-segment structure on the micro-phase separation of TPUs has been widely investigated in chemistry and technology of polyurethanes, because polyols are made with a range of architectures and backbones that can be tailored based on desired requirements [6]. The existence of a broad range of bifunctionally terminated soft segment such as synthetic and bio-based polyols offers endless potential for the design and synthesis of TPUs with controlled micro-phase morphologies [7]. Through theoretical and experimental studies, a number of research groups have reported on the effect of soft-segment structure on the properties of TPUs [8].

In a pioneering work, Petrovic and Javni have used the Flory–Huggins interaction parameter (χ) to study the effect of soft-segment length and concentration on phase

✉ Vahid Haddadi-Asl
haddadi@aut.ac.ir

[1] Department of Polymer Engineering and Color Technology, Amirkabir University of Technology (Tehran Polytechnic), Tehran, Iran

Published online: 01 March 2019

separation in segmented polyurethanes [9]. Results have shown that phase separation of block polymers cannot be elucidated based on a single function from χ. Many research groups have revealed that the product of Flory–Huggins interaction parameter and degree of polymerization quantifies the strength of separation between chemically unlike blocks [10]. Besides some theoretical approaches, numerous experimental techniques have been used to study the micro-phase separation including spectroscopy, thermal, rheology, scattering, and microscopy analyses [11]. Although these experimental methods have been successful, opportunities still exist to predict how changes in segments structure will affect the micro-phase separation behavior [12]. In the last decades, the interest in simulation and prediction of material properties has grown considerably due to their potential applications both in academia and industry [13]. Simulation and prediction of polyurethane properties, such as micro-phase separation, not only help to understand the underlying molecular mechanisms but also can reduce time and energy needed for experimental works. Molecular dynamics (MD) simulation is one of the most successful and widely applicable approaches to study the interaction between atoms and to explore the statistics and the dynamics of a system in equilibrium [14]. It acts as a link between microscopic scale and the macroscopic world of the laboratory [15]. Dynamic properties of a system-like time-dependent responses to perturbations, spectral, transport coefficients and rheological properties could be obtained with MD simulation. Unfortunately, only a few such investigations have so far been focused on the micro-phase separation of polyurethanes and many aspects yet have not been clarified [16]. For instance, Tao et al. have predicted the phase-separated structures of polyurethanes by calculating the interaction energy parameter and terms between hard and soft segments [17]. Madkour and Azzam have used the MD simulation to study the self-assembly of thermoplastic polyurethane elastomers [18]. They have reported the remarkable loss in the entropy showing much lower values for the self-diffusion coefficients of the self-assembly hard blocks due to the restriction in their mobility. The influence of fluorine on micro-phase separation in fluorinated polyurethanes have been studied by Wang et al. The MD simulation results have shown that increasing fluorine content of soft segments enhances hydrogen-bond interactions among soft and hard segments and thereby reducing the degree of micro-phase separation [19]. Recently, by calculating the intersegmental interactions between hard and soft segments, Avaz et al. have proposed that polyethylene oxide length could control phase separation of segmented polyurethane in a binary solvent [20].

Since the micro-phase separation of polyurethanes has been recognized as an important parameter, clarifying new methods to quantify micro-phase separation could be a great achievement. Hence, the goal of this work was based on experimental, theoretical and computational approaches to investigate the effect of soft-segment architecture on the micro-phase separation of TPUs. For this purpose, the MD simulation was used to evaluate the polymer interactions at atomic level. Then, the synthesized samples were evaluated by attenuated total reflectance Fourier transform infrared (ATR-FTIR) spectroscopy, atomic force microscopy (AFM), dynamic mechanical/thermal analysis (DMTA), differential scanning calorimetry (DSC), stress–strain curves and rheometric mechanical spectrometry (RMS). Experimental observations, physical–chemistry calculations and results from MD simulation were compared and evaluated.

Experimental

Materials

Poly(tetramethylene ether) glycol (PTMG) (M_n 1000 and 2000 g/mol), polycaprolactone diol (PCL-diol) (M_n 500 and 2000 g/mol), 4,4′-diphenylmethane diisocyanate (MDI), 1,4-butanediol (BDO) were purchased from Sigma–Aldrich. *N,N*-Dimethylacetamide (DMAC) was obtained from Merck.

Synthesis of TPU

TPU was synthesized by a two-step solution polymerization method. Polymerization was carried out into a two-necked round-bottomed flask equipped with a vacuum inlet tube and a raw material entrance. The reaction assembly was placed in a heating oil bath. Prior to mixing, PCL, PTMG, MDI, and BDO were dried in a vacuum oven at 80 °C for 4 h to ensure residual moisture removal. For polyurethane synthesis, the molar ratios of polyol, MDI, and BDO were determined [Fig. 1, a triangular profile diagram presenting the ratio of components, i.e., polyol (p), diisocyanate (i) and chain extender (c)]. Detailed information on the synthesized polyurethanes is presented in Table 1. Briefly, polyol with DMAC was added to the flask. Later on, MDI was added into the mixture and reacted with polyol for 3 h at 75–85 °C under continuous stirring to render a macrodiisocyanate prepolymer. In the chain extension step, BDO was added to the prepolymer. During this step, the viscosity of polyurethane was slowly increased due to the ongoing chain-extension reaction. After 3 h reaction, the obtained viscous liquid was poured into a preheated silicone mold and placed in an oven at 85 °C for 24 h. Finally, all samples were removed from the mold and stored at ambient temperature.

Characterization

Infrared spectra of the TPU samples were recorded on a attenuated total reflectance Fourier transform infrared

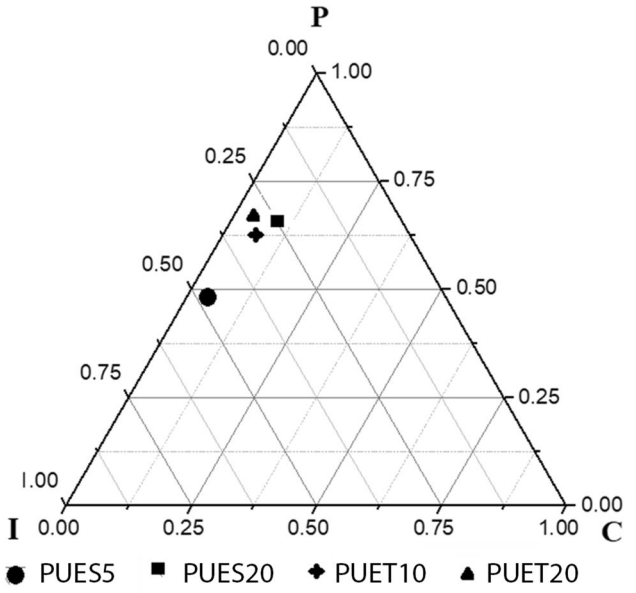

Fig. 1 Triangle diagram for polyurethane synthesis. *P* polyol, *I* isocyanate, *C* chain extender

spectroscopy (ATR-FTIR; Nexus 670, Nicolet) in the range between 4000 and 400 cm^{-1}, with a resolution of 0.1 cm^{-1}.

Gel permeation chromatography (GPC) was carried out with a Young Instrument Co. (Korea) unit using a 50,000–600,000 column.

Atomic force microscopy (AFM) was performed with a Dualscope/Rasterscope C26 (DME, Denmark) equipment in tapping mode on the thin-film samples at room temperature. AFM images were processed using data processing software.

Differential scanning calorimetry (DSC) experiments were conducted with a Flash DSC 1 of Mettler-Toledo, to evaluate the thermal properties of TPU samples. The experiments were conducted at a constant heating rate of 10 °C/min on samples (15–20 mg) packed in aluminum pans under nitrogen flow.

Density of the synthesized TPUs was measured using a densitometer. This instrument can measure the density of different polymeric materials such as thermoplastics, thermosets, elastomers and even light metals. The densitometer measures density through a density gradient column approach. This approach compares the densities of test samples with those of known density values. The densitometer is composed of two columns which are filled with test sample, thermostatic fluids and glass balls of known density. The working range for densitometer is from 0.5 to 3 g/cm^3.

Dynamic mechanical properties of the TPU samples were measured using dynamic mechanical thermal analyzer (Diamond DMA; Perkin & Elmer) in the tensile mode, heating rate of 5°C/min, frequency of 1 Hz and static force of 0.1 N on the molded samples (20 × 11 × 1 mm).

Table 1 Detailed information on the synthesized polyurethanes

Sample designation	Composition (mol%) polyol/MDI/BDO	Soft-segment molecular weight (g/mol)	M_n (g/mol)	M_w (g/mol)	PDI	N	H (pa s)	R_g (nm)	DSC T_{mhs} (°C)	DMTA T_{gss} (°C)	DMTA T_{ghs} (°C)
PUES5	1/ 2/ 1	PCL-500	40,891	56,429	1.38	97	332	9	149	− 29	76
PUES20	1/ 3/ 2	PCL-2000	131,602	169,766	1.29	1128	178	16	160	− 47	60
PUET10	1/ 2/ 1	PTMG-1000	84,985	132,577	1.56	1264	167	13	143	− 45	78
PUET20	1/ 3/ 2	PTMG-2000	111,000	158,730	1.43	135	147	15	165	− 48	98

Tensile properties of the samples were measured using a tensile testing machine. Tensile-dumbbell specimens for tensile tests (according to ASTM D 638 type V) were prepared from compressed films using appropriate punch. Tensile tests were carried out at room temperature using a Galdabini universal mechanical testing machine (Model Sun 2500) with a crosshead speed of 40 mm/min.

To measure the linear viscoelastic responses of TPUs, a rheometric mechanical spectrometer (PaarPhysica UDS200), equipped with a parallel plate fixture (25 mm diameter and a constant gap of 1 mm), was employed. The TPUs were heated for 15 min to erase thermal history, residual stress, and hard domains in melting temperature. The samples were cooled rapidly to the annealing temperature. This cooling process usually took 2 min for 50–70 °C drops in temperature. Next, the storage modulus and the loss modulus (G', G'') of the samples were measured by a time-sweep experiment to study the micro-phase separation and hard domain aggregation, at an annealing temperature for 2 h.

Computational methodology

MD simulations were carried out with the commercial molecular modeling software package Materials Studio 4.3 from Accelrys Software Inc. (San Diego, CA, USA). For computing interatomic interactions, the COMPASS (condensed-phase optimized molecular potentials for atomistic simulation studies) force field was selected. It is worth noting that the COMPASS force field has been already applied to a wide range of polymers such as PCL, PTMG and polyurethane [21]. First, PCL, PTMG, MDI and BDO repeat units were created, then based on experimental molecular design, TPUs were generated in different soft segments by module building. In the next step, cubic simulation boxes were constructed using amorphous cell module, structural schemes of synthesized TPUs and simulation boxes, as shown in Fig. 2. Properties of the simulation boxes are collected in Table 2. The TPU systems are in a quite high-energy state, hence minimizations should be performed to remove undesirable interactions and to attain the lowest energy level. For this purpose, TPU chains were optimized by the steepest

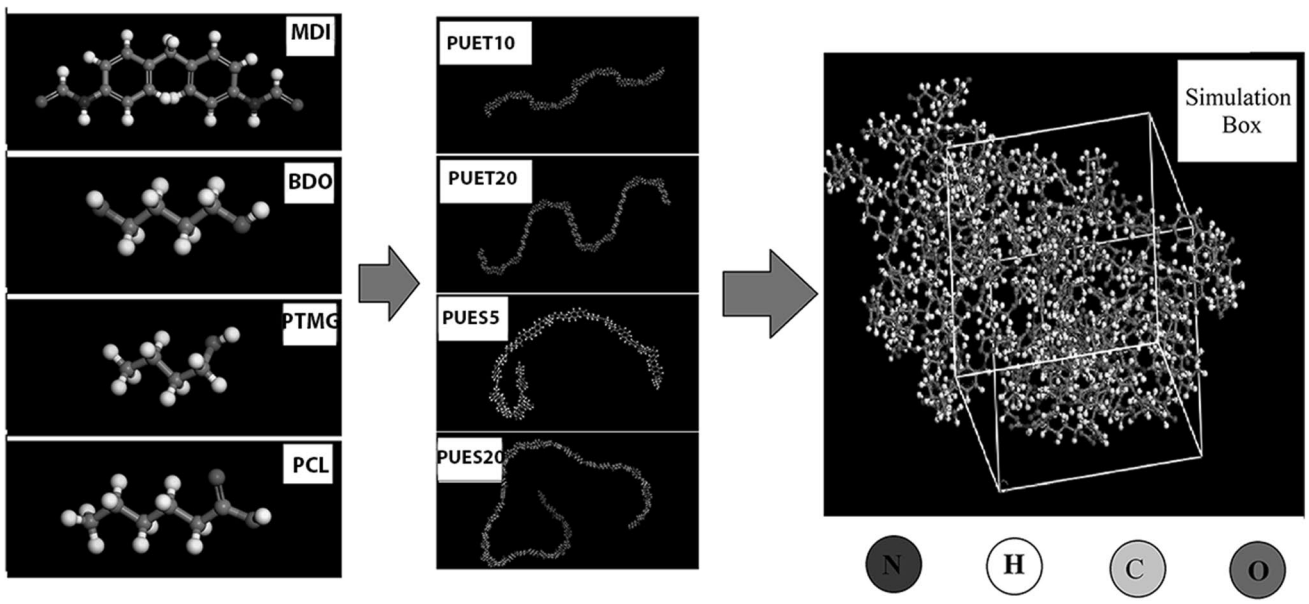

Fig. 2 Schematic of molecular chain and amorphous cell

Table 2 Detailed information on the simulated polyurethanes

Simulated system	Initial MD box length (nm)	Final MD box length (nm)	Soft-segment repeat unit	Hard segment repeat unit	χ_{MD}	δ_{MD} (J/cm^3)$^{0.5}$	D_{MD} of hard segments (10^{14}m^2/s)	C_∞	L_P
PUES5	4.55	2.89	8	8	7.02	12.26	6.872	5.46	4.96
PUES20	5.65	3.61	8	8	13.7	12.85	5.039	5.12	4.85
PUET10	4.62	2.92	8	8	14.04	11.067	6.727	4.94	4.66
PUET20	5.06	3.28	8	8	23.3	11.042	3.868	5.01	4.81

descent and conjugate gradient method (the maximum number for minimization was 20,000). Periodic boundary conditions were performed by providing the TPU system state as framed around by its facsimiles and represent the TPU chains in bulk. MD simulations were conducted for 1000 picosecond (ps) at *NPT* (constant pressure *P* and constant temperature *T*) condition until the box size became constant and then using *NVT* (constant volume *V* and constant temperature *T*) condition to reach its equilibrium at 1000 ps, where the temperature and pressure were controlled by the Anderson thermostat (298 °K) and Berendsen barostat (0.0001 GPa), respectively. The attained module was used for minimization and dynamic parts. The integration of the equations of motion has been performed by means of Verlet velocity time integration method with a time step of 1 femtosecond (fs). The initial velocities of the atoms were assigned using a Maxwell–Boltzmann distribution at the desired temperature and pressure. A cut-off radius of 1.25 nm was used for Lennard-Jones interactions and Ewald summation to compute long-range electrostatic interactions.

Results and discussion

To study the effect of soft-segment architecture on the micro-phase separation of TPUs, four TPU types have been synthesized in this work. Based on selection of ether and ester type polyols with different molecular weights, chemistry of TPUs would be different. The chemical structure of the TPUs was investigated by ATR-FTIR analysis. There is a wide range of molecular interactions such as hydrogen bonding, dipole–dipole, and induced dipole–dipole interactions between hard segments that strongly affect the micro-phase separation of TPUs. Figure 3 illustrates ATR spectra of the synthesized samples. The characteristic peaks of synthesized TPUs are in line with the other reports in the literature [22]. The obtained results confirm the successful polymerization of all samples. One distinguishable phenomenon is the relatively short distance and parallel orientation between the aromatic rings in hard segments. The π–π interactions can be detected in ATR spectra. The peak at 1600 cm^{-1} corresponds to the aromatic ν(C=C) vibration [23]. As it is depicted in Fig. 3, the highest and lowest intensity of the π–π interactions peak belongs to PUET20 and PUES5 samples, respectively. In this study case, the intensity of π–π interactions could be an indication of micro-phase separation of TPUs. The intermolecular interactions (including hydrogen bonding, van der Waal's interactions, etc.) of polyurethane chains can be investigated using the pair correlation function, denoted by $g(r)$ [24]:

$$g_{AB}(r) = \frac{1}{\rho_{AB} 4\pi r^2} \frac{\sum_{i=1}^{K} \sum_{j=1}^{N_{AB}} \Delta N_{AB}\left(r \to r + \delta_r\right)}{N_{AB} \times K}, \quad (1)$$

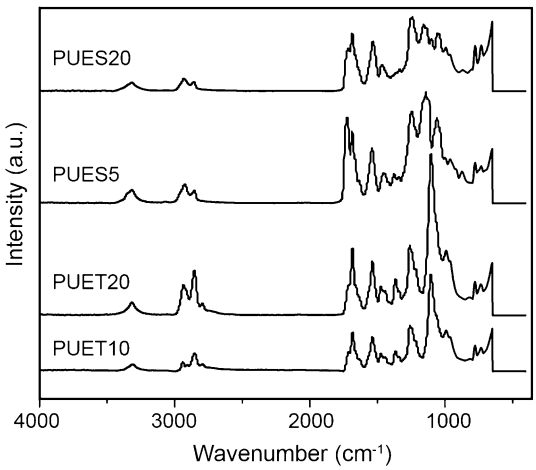

Fig. 3 ATR-FTIR spectra of synthesized TPUs

where N_{AB} is the total number of atoms *A* and *B* in the system, *K* is the number of time steps, δ_r is the distance interval, ΔN_{AB} is the number of *B* (or *A*) atoms between *r* and δ_r around an *A* (or *B*) atom, and ρ_{AB} is the bulk density. The radial distribution function (RDF) $g(r)$ represents the probability of finding a pair of atoms at a distance *r* with respect to the bulk phase in a completely random distribution. On the other hand, $g(r)$ reflects the relative concentration of molecules as a function of distance *r* from a given molecule [24]. The configurations and relative positions of the TPU chains in the simulation trajectory were carefully checked. After analyzing the molecular dynamics simulation results, the pair correlation functions of these systems, $g(r)$, were obtained. To this end, the RDF between carbon atoms in aromatic rings of hard segments was calculated (Fig. 4). The results indicate that the first peak which belongs to PUES20 appears sooner and it is higher than that of PUES5. The first peak of the former is appeared around 0.2 nm, while the latter has not any peak in this region. This indicates that in PUES20, the hard segments attract each other more favorably and their short-range interactions are higher than those of PUES5. On the other hand, the packing structure formed between PUES20 hard segments is relatively high and the strongest interaction has occurred at the closest distance. Greater interactions between the hard segments lead to the formation of more separated hard segments in PUES20 against no such strong separations in PUES5. As shown in Fig. 4, the first peak intensity around 0.2 nm is higher in PUET20, suggesting strong interaction between aromatic rings in PUET20. Although PUET10 shows the peak at around 0.2 nm, its intensity is lower than that of PUET20. The results indicate that the difference in peak intensity (at same position) is related to the packing of hard segments and thereby the sample with greater intensity has more packing structure. It has to be noted that Fig. 4 indicates that the main

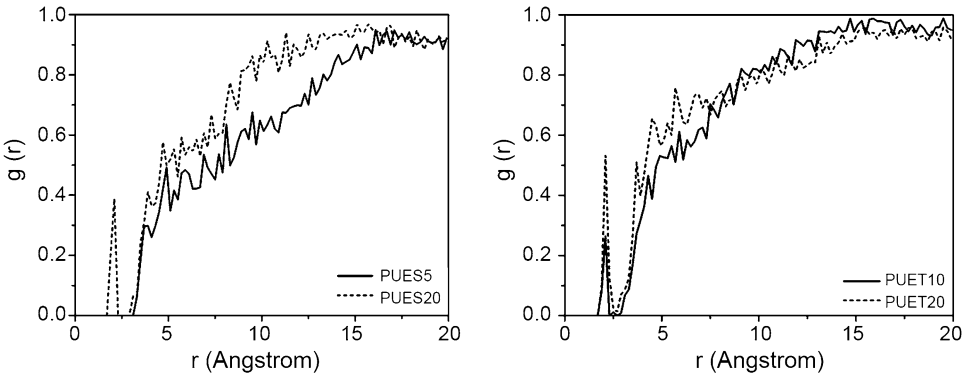

Fig. 4 Radial distribution functions between carbon atoms in aromatic rings of hard segments

first peak takes place around 0.46 nm (second peak) which clearly shows the average distance between TPU chains and the first peaks around 0.2 nm contain the interactions between carbon atoms in aromatic rings of a hard segment. It can be concluded that with increasing soft-segment length, the π–π interactions, and therefore, micro-phase separation of samples would be improved. These observations are consistent with the ATR-FTIR results.

It is fully known that the free C=O stretching stems from the mixed hard and soft segments, while the bonded C=O arises from hydrogen bonded in hard domains having aligned urethane linkages [25]. The ATR-FTIR spectrum of PUET20 shows a dominant hydrogen-bonded C=O absorbance at 1701 cm^{-1} (Fig. 3). The replacement of the shorter soft segment (PTMG-1000) with PTMG-2000 leads to a less hydrogen-bonding structure. Changes in the hydrogen-bonded intensity based on alternation in soft-segment length are more clearly observed in PCL-based samples. The hydrogen-bonded C=O stretching near 1701 cm^{-1} is reduced in intensity as PCL-500 is substituted with PCL-2000.

Based on the two absorption peaks located at 1725 and 1701 cm^{-1}, corresponding to the free and hydrogen-bonded C=O stretching, respectively, the degree of micro-phase separation (DPS_{ATR}) can be calculated by the following equation:

$$DPS_{ATR} = \frac{C{=}O_{bonded}}{C{=}O_{bonded} + C{=}O_{free}}, \quad (2)$$

where $C{=}O_{bonded}$ and $C{=}O_{free}$ are the intensities of characteristic absorbance at 1701 cm^{-1} and 1725 cm^{-1}, respectively. Based on the ATR-FTIR spectra, the DPS_{ATR} of the samples was calculated (Fig. 5). The degree of micro-phase separation for PUET20 and PUES20 was much higher than that for other two samples. Segmental incompatibility in the TPUs rises by increasing soft-segment length. The PUET20 has the highest DPS_{ATR} (64%). As the PTMG has lower polarity than the PCL, the degree of micro-phase separation is more noticeable due to the high thermodynamic incompatibility of the soft and hard segments. Results from Fig. 5 show that the minimum degree of micro-phase separation of the synthesized samples belongs to PUES5 (45%). Obviously, incorporation of shorter soft segments promotes phase mixing, while incorporation of longer soft segments encourages phase demixing. The molecular characteristics of the four block polymers employed in this study are summarized in Table 1. Based on GPC results, the polydispersity of the samples is almost constant around 1.3–1.5 with different polyol type and molecular weight. This is an indication that no side reactions occurred during reactions [26]. These polyurethanes show an increase in melting temperature with an increase in soft-segment length. The PUES5 and PUET10 have melting points of 149 and 143 °C, respectively. With increasing polyol molecular weight, the melting temperature of polyester- and polyether-based polyurethanes have increased by about 11 and 22 °C, respectively.

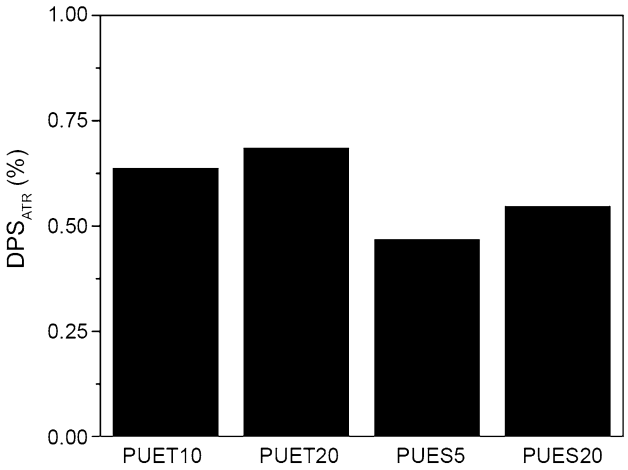

Fig. 5 $DPS_{ATR-FTIR}$ of synthesized TPUs

One of the best ways to predict phase compatibility in block polymers is based on solubility parameters compared in both blocks and the calculation of interaction

parameters [27]. The thermodynamic interaction parameter (χ) of hard and soft segments in TPUs can be expressed by

$$\chi = \left(V_r/RT\right)\left(\delta_{ss} - \delta_{hs}\right)^2, \tag{3}$$

where V_r is the molar volume of TPU repeat unit, R and T are the universal gas constant and temperature, respectively. δ_{ss} and δ_{hs} are the Hansen solubility parameters of the soft and hard segments, respectively. Hansen solubility parameter can be expressed in terms of the individual solubility parameters δ_d, δ_p, and δ_h [27]:

$$\delta = \sqrt{\delta_d^2 + \delta_h^2 + \delta_p^2}, \tag{4}$$

where δ_d, δ_h, and δ_p are Hansen parameter contribution from dispersion, hydrogen bond, and polar forces, respectively. With the aid of Hoftyzer and van Krevelen method, the individual solubility parameters are estimated as [27]

$$\delta_d = \frac{\sum F_{di}}{V}, \quad \delta_p = \frac{\sqrt{\sum F_{pi}^2}}{V}, \quad \delta_h = \sqrt{\frac{\sum E_{hi}}{V}}, \tag{5}$$

F_{di}, F_{hi} and E_{hi} are the components for calculation of singular solubility parameters, which are available in literature for functional groups. The critical thermodynamic interaction parameter can be calculated by means of the following equation [27]:

$$\chi_{crit} = \frac{1}{2}\left(\frac{1}{\sqrt{x_{ss}}} + \frac{1}{\sqrt{x_{hs}}}\right)^2, \tag{6}$$

where x_{ss} and x_{hs} designate the numbers of soft and hard segments, respectively. In an atomistic simulation, the cohesive energy density (CED) is defined as the increase in energy per mole of a material when all intermolecular forces are eliminated. The E_{CED} corresponds to the cohesive energy per unit volume, i.e., the energy difference between a molecule in vacuum state and in the bulk amorphous state within a unit volume. It is a measure of the intermolecular forces, which is estimated through the non-bonded van der Waals and electrostatic interactions [28]:

$$E_{CED} = \frac{\left(U_{vdw} + U_Q\right)}{V}, \tag{7}$$

where U_{vdw} and U_Q are van der Waals and electrostatic energy, respectively. Therefore, the molecular dynamic solubility parameter (δ_{MD}) can be measured [28]:

$$\delta_{MD} = \sqrt{E_{CED}}. \tag{8}$$

We have also calculated the interaction parameter from molecular dynamics simulation by [28]

$$\chi_{MD} = \frac{z\Delta\varepsilon}{kT}, \tag{9}$$

where z is the lattice coordination number and $\Delta\varepsilon$ is the excess exchange interaction energy. At a glance, the calculated values for δ parameters in PTMG-based samples are lower compared to PCL-based polyurethanes (Table 3). The δ for PUET10 is 20.2 $(J/cm^3)^{0.5}$, as against 20.03 $(J/cm^3)^{0.5}$ for PUES20. This could be explained by the fact that, at equal soft-segment concentration, the increase in polyol molecular weight leads to formation of less urethane linkages. Solubility parameter of urethane group, 37.2 $(J/cm^3)^{0.5}$, is quite high when compared with common soft segments, which are usually in the range of 15–20 $(J/cm^3)^{0.5}$. The main conclusion to be drawn from molecular dynamics solubility parameters (Table 2) is that, the δ_{MD} is high for PUES5 and PUES20 in comparison with PTMG-based samples which are consistent with the calculated results. Calculated χ parameters for different synthesized samples are given in Table 3. The values of χ and χ_{MD} in all samples are above this critical value, indicating the immiscibility of the systems. As seen, χ parameter of PTMG-based TPUs is approximately 6 times higher than others. It should be noted that calculated χ parameters do not change with increasing polyol molecular weight. It might be due to the fact that χ parameter is calculated based on enthalpic approach and entropy of the chains has not been accounted. In addition, change in the segment length does not play a key role in solubility parameter calculations. Consequently, to consider the role of entropy in predicting the micro-phase separation behavior, we will focus on the product of interaction parameter and degree of polymerization (χN). By increasing the N, entropy related with a single chain increases intensely due to the large number of different conformations which a chain can adopt [29]. To simplify the matter, two approaches are studied to analyze the micro-phase separation here; enthalpic and entropic. The χ represents the enthalpic factor and

Table 3 Calculated interaction parameter and solubility parameter

Sample	χ	χ_{crit}	δ_{ss} $(J/cm^3)^{0.5}$	δ_{hs} $(J/cm^3)^{0.5}$	δ_d $(J/cm^3)^{0.5}$	δ_p $(J/cm^3)^{0.5}$	δ_h $(J/cm^3)^{0.5}$	δ $(J/cm^3)^{0.5}$
PUES5	0.215	0.147	21.7	22.93	19.1	3.16	7.71	20.83
PUES20	0.215	0.0841	21.7	22.93	18.53	1.93	7.38	20.03
PUET10	1.34	0.0995	19.36	22.93	19.07	2.96	6	20.2
PUET20	1.34	0.0712	19.36	22.93	18.86	2.26	5.92	19.89

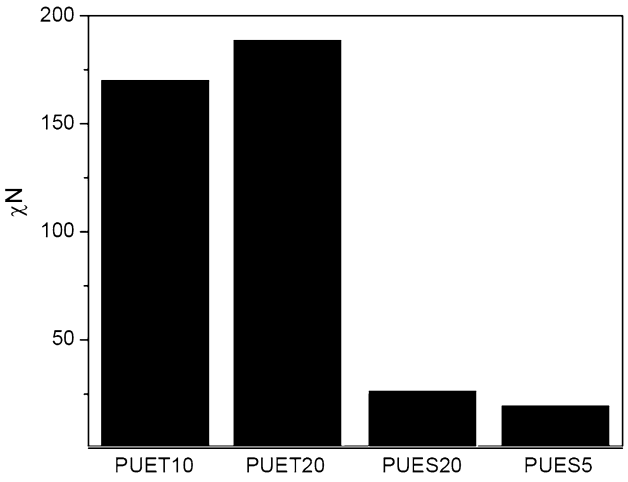

Fig. 6 χN of synthesized TPUs

the N contains chain entropy. It is worth bearing in mind that these separated factors cannot be accounted for phase behavior. Figure 6 illustrates the χN for all samples. As seen from this figure, the minimum χN of the synthesized samples belongs to PUES5, precisely 20.91. In contrast, PUET20 has the highest χN (181.8) compared to others. Samples synthesized using higher molecular weights of soft segment show greater micro-phase separation due to lower entropy of mixing contribution, implying coarse mixing between the hard and soft segments.

Figure 7 shows the density values measured experimentally and by simulation. The experimental density has been measured with a soaking method. The experimental and theoretical values are approximately the same for PUET20 and PUES20. The results exhibit that PUES5 has the maximum density, since it possesses lower content of polyurethane short chains compared to other TPUs. Whereas, PUET20 reveals the minimum density because of folding and flexibility of polymer chains in this configuration. The density of TPUs, obtained by simulation, is in good agreement with the experimental value obtained from experimental study.

Furthermore, according to following relations and MD data, chain stiffness (C_∞) and persistence length (L_p) of samples have been calculated. Calculated parameters for different synthesized samples are given in Table 2:

$$\Gamma =< \mathrm{Cos}\,\phi >= \frac{\mathrm{Cos}\,\phi_1 + \sum_{i=2}^{n} e^{-\Delta E_i/kT}\,\mathrm{Cos}\,\phi_i}{1 + \sum_{i=2}^{n} e^{-\Delta E_i/kT}}, \tag{10}$$

$$C_\infty = \frac{1+\Gamma}{1-\Gamma}\frac{1+\cos\theta}{1-\cos\theta}, \tag{11}$$

$$l_p = l_0\left[5\exp\left(-\frac{\Delta U}{KT}\right)+4\right]/\left[6\exp\left(-\Delta U/KT\right)\right], \tag{12}$$

where C_∞ and L_p are indicative of polyurethane chain stiffness. Polyester-based TPUs due to stronger polarity of the soft segment and more interactions reveal higher value of C_∞ and L_p which are in accordance with other experimental data.

Figure 8 shows the DSC results obtained from the cooling cycle of the samples prepared by quenching and annealing scanned from 200 to − 50 °C. The PUET20 exhibits exothermic peak at approximately 100 °C, corresponding to crystallization of hard segments. The PUES5 shows a low temperature peak at approximately 50 °C. As it may be seen from the exothermic curves, the sample with more thermodynamic incompatibility has more tendency to form crystals. These

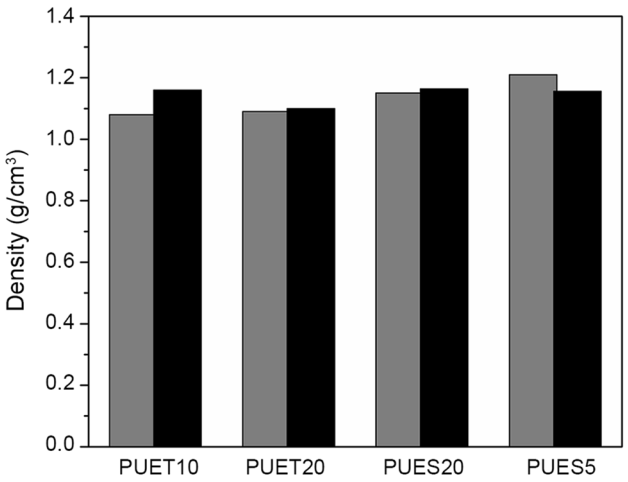

Fig. 7 Density of synthesized TPUs

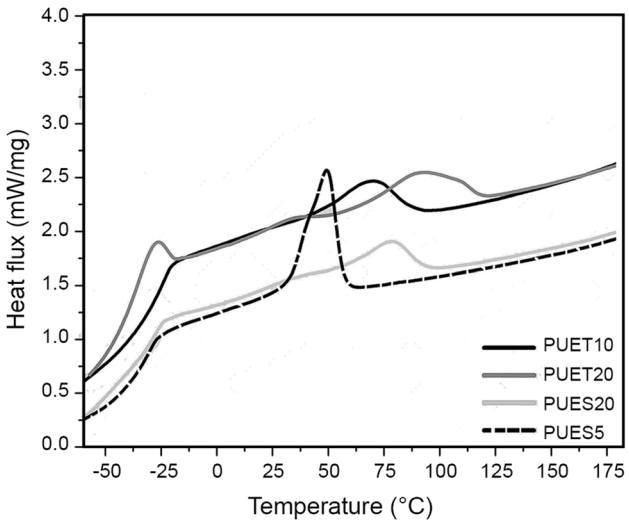

Fig. 8 DSC thermograms of synthesized TPUs

results clearly suggest that the incorporation of ether-based polyols substantially increases the rate of crystallization of the hard segments. Quantitative thermal analysis is one of the best ways to study the micro-phase separation of TPUs. To this end, we first have used f_{ss} which is the weight fraction of the soft segments in the soft-segment-rich phase [30]:

$$f_{ss} = \frac{\alpha\left(T_{g,hs} - T_g\right)}{\left(T_{g,ss} - T_g\right) + \alpha\left(T_{g,hs} - T_g\right)}, \tag{13}$$

where $T_{g,ss}$ and $T_{g,hs}$ are the glass transition temperature of the pure soft and hard segments, respectively, and $\alpha = \Delta C_{p,hs}/\Delta C_{p,ss}$. $\Delta C_{p,ss}$ and $\Delta C_{p,hs}$ are change in heat capacity at the glass transition of the pure soft and hard segments, respectively [30]:

$$T_g = \frac{w_{ss}T_{g,ss} + \alpha w_{hs}T_{g,hs}}{w_{ss} + \alpha w_{hs}}. \tag{14}$$

Here w_{ss} and w_{hs} are the soft and hard segment weight fractions in the samples. Several equations are targeted to define the relation between the glass transition of the pure components and the glass transition of the corresponding homogeneous mixed phase in polymers. Fox equation is one of the most general empirical forms [30]:

$$\frac{w_{ss} + kw_{hs}}{T_{g,mp}} = \frac{w_{ss}}{T_{g,ss}} + \frac{kw_{hs}}{T_{g,hs}}, \tag{15}$$

where k as Wood constant was taken as unity in the original treatment by Fox. Another equation which can determine the glass transition of the homogeneous mixed phase in TPUs was proposed by Chen et al. [31]:

$$T_{g,mp} = w_{ss}T_{g,ss} + w_{hs}T_{g,hs}. \tag{16}$$

In attempting to use Eq. 14 which has been previously used by Cooper et al. to calculate f_{ss}, an interesting point was found [30]. Once the T_g from Eq. 14 was substituted in Eq. 13, it resulted in $f_{ss} = w_{ss}$. We can solve this problem using T_g from Eqs. 15 and 16 and also DMTA analysis. The calculated values are listed in Table 4. The results show that with increasing soft-segment molecular weight, f_{ss} shows an increasing trend. PUET20 and PUES5 have the highest and the lowest f_{ss}, respectively. In samples with high micro-phase-separated structures, the soft segments have more freedom to move. Hence, these polyurethanes have lower T_g of soft segments compared with those of greater phase mixing of hard and soft segments, leading to high weight fraction of the soft segments embedded into the soft-segment-rich phase. The main conclusion to be drawn from the results is that f_{ss} is a kind of representation for degree of micro-phase separation in polyurethanes. This outcome is in very good agreement with the findings stated in previous sections. The degree of segregation (α_{seg}) was calculated from the jump in specific heat capacity at T_g using the DSC analysis [32]:

$$\alpha_{seg} = \left[\frac{\Delta C_{p,ss}}{\left(\Delta C_{p,olig} w_{ss}\right)}\right] K_s, \tag{17}$$

where $\Delta C_{p,olig}$ is the change in heat capacity at the glass transition of polyols and K_s value depends on the repeating units of TPU and changes in 0.63–0.68 interval. Vilensky and Lipatov have shown that the values of α_{seg} calculated from Eq. 17 are in line with the same parameter estimated from SAXS analysis [32]. The measured properties and the results of these calculations are presented in Table 4. Again, PUET20 and PUES5 have the highest and the lowest α_{seg}, respectively. These results indicate that this approach is in line with other ways for studying micro-phase separation performance.

As shown in Fig. 9, it is evident that the samples with polyester soft segments possess higher modulus compared with those of polyether soft segments (due to greater polarity of

Table 4 Quantitative thermal analysis parameters

Sample	f_{ss} based on Eq. 15	f_{ss} based on Eq. 16	f_{ss} based on DMTA T_g	α_{seg}
PUES5	0.4561	0.39	0.408	0.43
PUES20	0.6696	0.617	0.490	0.48
PUET10	0.6395	0.546	0.435	0.73
PUET20	0.6819	0.59	0.542	0.84

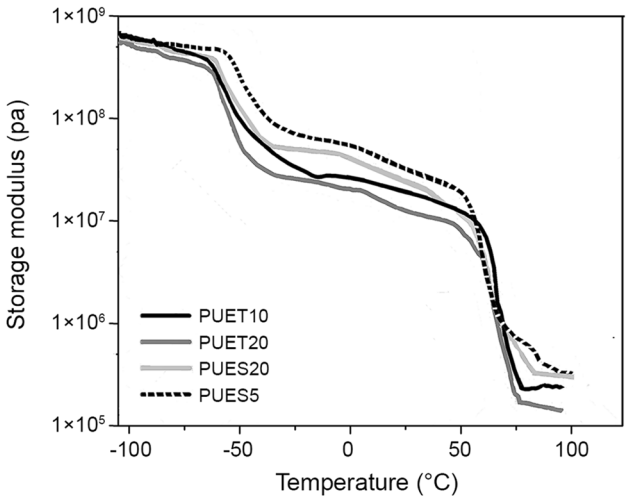

Fig. 9 Temperature dependence of the dynamic viscoelasticity of synthesized TPUs

the soft segments in polyesters compared with polyethers). The PUET20 has the lowest initial modulus because of two reasons: first, it is composed of a polyether soft segment and second its soft segments are long thus conferring substantial flexibility to the sample. The PUES5 has represented the least phase separation as evidenced from the experimental analysis or calculating values. Since in this sample the soft and hard segments are highly intermixed, this sample has possessed the lowest temperature drop during thermal transitions. Compared to PUES5 sample, PUES20 displays more intense phase separation and thus more profound drop in modulus. When soft and hard segments are highly intermixed, an intense drop in modulus is avoided. Compared to PUET10 sample, PUET20 starts its drop earlier. This occurrence signifies that sample PUET20 has purer soft segment due to more phase separation. Furthermore, sample PUET20 shows more profound drop in modulus during thermal transitions. Besides, its modulus substantially decreases at elevated temperature due to destruction of hard segments.

Another important characteristic of the TPU system is the mobility of hard block units. The Einstein relationship is widely used for calculating diffusion coefficient from molecular dynamics simulation. When an atom undertakes random Brownian motion in a three-dimensional space, its self-diffusion coefficient can be calculated by limiting the slope of mean square displacement (MSD) as a function of time:

$$\mathrm{MSD}(t) = \frac{1}{N}\sum_{i=1}^{N}\left\langle \left| r_i(t) - r_i(0)\right|^2 \right\rangle, \tag{18}$$

$$D_{\mathrm{MD}} = \frac{1}{6N}\lim_{t\to\infty}\frac{d}{\mathrm{d}t}\sum_{i=1}^{N}\left\langle \left| r_i(t) - r_i(0)\right|^2 \right\rangle, \tag{19}$$

where $r(t)$ and $t(0)$ denote the position vector of the atom at time t and $t=0$, respectively. The angular brackets denote averaging of all choices of time origin within a dynamic trajectory. Based on the mean squared displacements of the four model polyurethanes, self-diffusion coefficients of hard block units could be calculated (Table 2). The results clearly show that the self-diffusion coefficients of the samples decrease with increasing the soft block length. The PUET20 and PUES5 have the lowest and the highest D_{MD}, respectively [33]. This indicates that great interactions in the PUET20 can retard the movement of hard segments and decrease its diffusion coefficient. The increase in the molecular interactions has resulted in a decrease in self-diffusion coefficients due to the increase in the short-range interactions and packing and thereby restricting chain movement.

To better understand the influence of soft-segment type and molecular weight on the micro-phase separation of TPUs, a detailed study based on compressible regular solution model was conducted [34]. According to the definition of reduced properties typically used in equation of state theories, reduced density could be measured:

$$\tilde{\rho}_i(T,P) = \frac{V_{\mathrm{hc},i}}{V_i} = \frac{\rho_i}{\rho_i^*}. \tag{20}$$

At this assumed hard core state, $V_{\mathrm{hc},i}$ and V_i are the total volume and the actual volume occupied by the pure compressible components at any temperature T and pressure P, respectively. ρ_i is the T- and P-dependent mass density and $\rho^*{}_i$ is the hard core density. The free volume of component i, $V_{\mathrm{f},i}$, is calculated by the difference between the total volume V_i at T and P and the hard core volume $V_{\mathrm{hc},i}$ [34]:

$$V_{\mathrm{f},i} = V_i - V_{\mathrm{hc},i} = \left(1-\tilde{\rho}_i\right)V_i, \tag{21}$$

$$V_{\mathrm{f,tot}} = V - V_{\mathrm{hc,ss}} - V_{\mathrm{hc,hs}} = (1-\tilde{\rho})V. \tag{22}$$

Combinatorial entropy of TPUs can be measured by [34]

$$\Delta S_{\mathrm{comb}}/K = -\left[n_{\mathrm{ss}}\ln\phi_{\mathrm{ss}} + n_{\mathrm{hs}}\ln\phi_{\mathrm{hs}}\right] + \left[n_{\mathrm{ss}}\ln\left(\frac{1-\tilde{\rho}}{1-\tilde{\rho}_{\mathrm{ss}}}\right) + n_{\mathrm{hs}}\ln\left(\frac{1-\tilde{\rho}}{1-\tilde{\rho}_{\mathrm{hs}}}\right)\right], \tag{23}$$

where ϕ_i is the volume fraction of component i (soft and hard segments). Change in interaction energy per unit volume, $\Delta E_{\mathrm{tot}}/V$, can be written in a formula that effectively separates the compressible and incompressible contributions to the change in interaction energy [34]:

$$\Delta E_{\mathrm{tot}}/V = \phi_{\mathrm{ss}}\phi_{\mathrm{hs}}\tilde{\rho}_{\mathrm{ss}}\tilde{\rho}_{\mathrm{hs}}\left(\delta_{\mathrm{ss},0}-\delta_{\mathrm{hs},0}\right)^2 + \phi_{\mathrm{ss}}\phi_{\mathrm{hs}}\left(\tilde{\rho}_{\mathrm{ss}}-\tilde{\rho}_{\mathrm{hs}}\right)\left(\delta_{\mathrm{ss}}^2-\delta_{\mathrm{hs}}^2\right), \tag{24}$$

$$\delta_i^2 = \tilde{\rho}_i\delta_{i,0}^2, \tag{25}$$

where $\delta_{i,0}$ is the solubility parameter at 25 °C. The change of Gibbs energy is given by [34]

$$\begin{aligned}\Delta g_{\mathrm{mix}} = kT\left[\frac{\phi_{\mathrm{ss}}\tilde{\rho}_{\mathrm{ss}}}{N_{\mathrm{ss}}v_{\mathrm{ss}}}\ln\phi_{\mathrm{ss}} + \frac{\phi_{\mathrm{hs}}\tilde{\rho}_{\mathrm{hs}}}{N_{\mathrm{hs}}v_{\mathrm{hs}}}\ln\phi_{\mathrm{hs}}\right] \\ + \phi_{\mathrm{ss}}\phi_{\mathrm{hs}}\tilde{\rho}_{\mathrm{ss}}\tilde{\rho}_{\mathrm{hs}}\left(\delta_{\mathrm{ss},0}-\delta_{\mathrm{hs},0}\right)^2 \\ + \phi_{\mathrm{ss}}\phi_{\mathrm{hs}}\left(\tilde{\rho}_{\mathrm{ss}}-\tilde{\rho}_{\mathrm{hs}}\right)\left(\delta_{\mathrm{ss}}{}^2-\delta_{\mathrm{hs}}{}^2\right),\end{aligned} \tag{26}$$

where v_{ss} and v_{hs} are the average soft and hard segmental volumes, respectively. Based on these equations, physicochemical characteristics of the samples are discerned and data are summarized in Table 5. Crucially, it was claimed that the Δg_{mix} is approximately equal to $\Delta E_{\mathrm{tot}}/V$ [34]. The data from Table 5 show that the Δg_{mix} of the PTMG-based TPUs is higher than that of polyester-based samples. It means that high immiscibility of the polyether soft and hard segments leads to great micro-phase separation. On the other

Table 5 Calculated parameters for compressible regular solution model

Sample	$\tilde{\rho}$	$V_{f,i}$	$V_{f,m}$	ΔS_{comb} (J/K)	$\Delta E_{mix}/V$ (J) $\approx \Delta g_{mix}$ (J)
PUES5	0.81	0.20	0.19	0.1518	1.7
PUES20	0.795	0.19	0.205	0.3067	2.23
PUET10	0.754	0.28	0.246	0.2319	3.4349
PUET20	0.737	0.29	0.262	0.3514	5.045

Table 6 Mechanical properties of polyurethane samples

Sample	PUET10	PUET20	PUES20	PUES5
Strength(Mpa)	15 ± 1	43 ± 2	46 ± 2	58 ± 2.5
Strain(%)	623 ± 80	648 ± 90	500 ± 70	472 ± 70
Modulus(Gpa)	0.78 ± 0.05	0.75 ± 0.0.4	0.809 ± 0.05	0.84 ± 0.06

hand, with increasing soft-segment molecular weight, Δg_{mix} increases almost by twofold.

Rheology is a trustworthy method deducing the micro-phase separation kinetics of TPUs. Intersection point of storage and loss moduli versus time curves is a critical point of the physical gel (cross time). The storage and loss moduli of the samples as a function of time are shown in Fig. 10. As evidenced from Fig. 10, the storage and loss moduli curves of PCL-based samples do not interrupt each other until 10000s. This means that these samples have slow micro-phase separation kinetics. Keen observation on the related image reveals that the storage and loss moduli of PUES20 are in closer distance compared to those of PUES5 which implies that this formulation has faster kinetics. The storage and loss moduli of the PTMG-based samples are also shown in Fig. 10. At a glance, cross time is observed in these samples. The cross time observed for PUET10 and PUET20 is 1610 and 730 s, respectively. Thus, the micro-phase separation kinetics is enhanced with increasing length of the soft-segment block (Table 6).

The morphology and structure of synthesized TPUs were also characterized by AFM. For polyurethanes, damage in contact mode AFM is well studied and hard to dodge. Tapping-mode AFM with phase detection is an additional opportunity for studying the polyurethane systems. Figure 11 presents the tapping-mode AFM images of the synthesized TPUs. The darker and brighter domains correspond to the soft and hard segments, respectively [35]. It is evident that the weight percentage observed for the hard domains of PUET20 is the highest. Replacement of the shorter soft segment with PTMG-2000 leads to formation of less hard domains. This trend was also observed for PCL-based TPUs as PCL-500 was substituted with high molecular weight PCL in the samples. The results corroborate that with increasing phase separation the hard domains in AFM images become more profound.

Ester-based TPUs show higher Young's moduli, whereas their elongation-at-break values are lower than those of ether-based samples (Fig. 12). The greater rigidity in ester-based TPUs arises from the rigid PCL chains as part of the main chain, while the flexibility appears from the overall flexibility of PTMG in ether-based TPUs [36]. Where hard segments are assembled in PUET20 causing higher tensile strength versus rather lower tensile strength observed in PUET10. Thus, micro-phase-separated domains and chain rigidity play a key role in escalation of Young's modulus and tensile strength [37].

Conclusion

In current research, the effect of soft-segment architecture on TPU properties has been investigated. To provide an easy-to-apply method for the prediction of the micro-phase separation of TPUs, physical–chemistry calculations and MD simulation were designed and evaluated. In "Experimental" section, TPUs based on PTMG (1000 and 2000 g/mol) or PCL (500 and 2000 g/mol), MDI, and BDO were synthesized. The spectroscopy and pair correlation function results showed that the highest and lowest intensity of

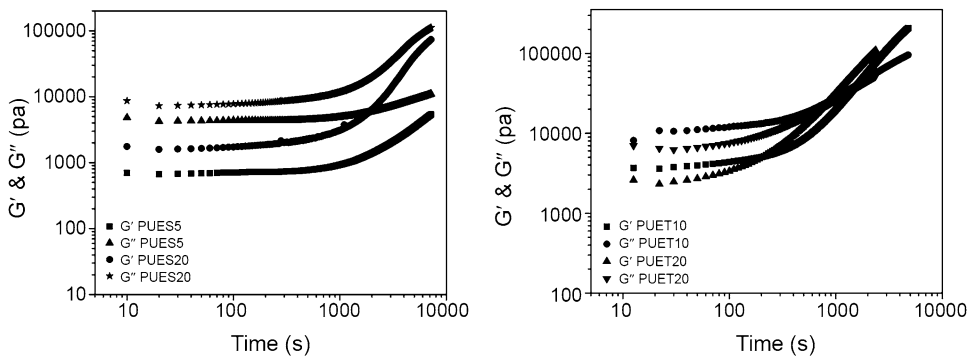

Fig. 10 Storage and loss moduli of synthesized samples as a function of time

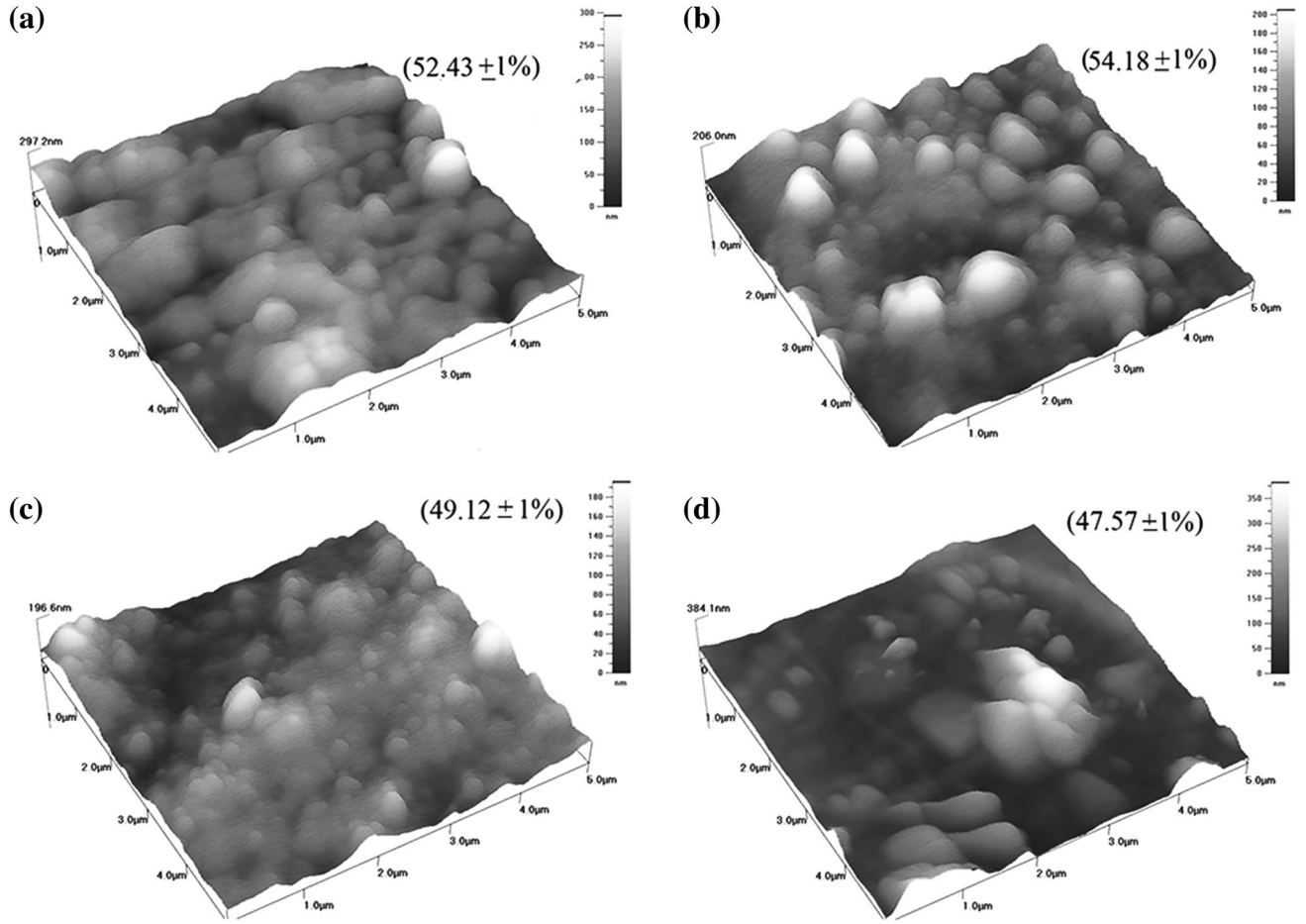

Fig. 11 Tapping-mode AFM images of synthesized TPUs: **a** PUET10, **b** PUET20, **c** PUES20, and **d** PUES5

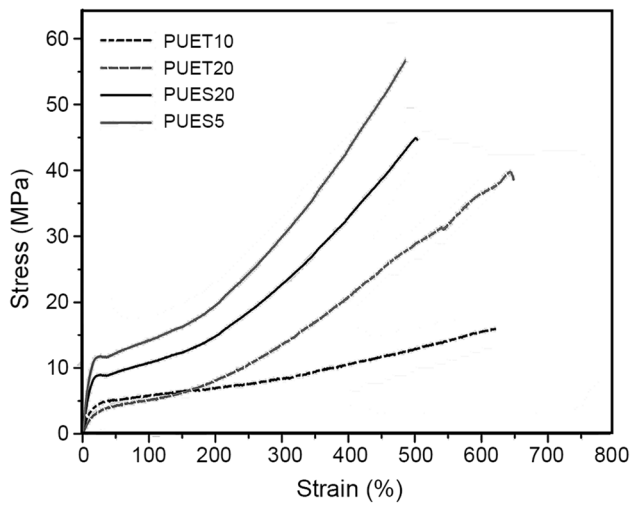

Fig. 12 Stress–strain curves of synthesized TPUs

the π–π interactions related peak belonged to PUET20 and PUES5, respectively. The values of χ and χ_{MD} in all samples were above the critical value, indicating the immiscibility of the systems. Calculated χN revealed that synthesized TPUs with higher molecular weight soft segment possessed higher micro-phase separation due to lower entropy of mixing contribution, implying coarse mixing between the hard and soft segments. Two parameters from thermal analysis (f_{ss} and α_{seg}) were utilized to measure the degree of micro-phase separation in TPUs. The increase of intermolecular interactions (high micro-phase separation) resulted in a decrease in MD self-diffusion coefficients due to increases in short-range interactions and packing and thereby restricting their movement and slowing down their self-diffusion. Based on pure component properties, compressible regular solution model showed that Δg_{mix} of the PUET20 was at the highest compared to other samples. Time-sweep tests revealed that PTMG-based TPUs possessed the fastest micro-phase separation kinetics. The main conclusion to be drawn is that all methods showed that the PUET20 and PUES5 have the highest and the lowest degree of micro-phase separation,

respectively. Moreover, in each class of polyol, the degree of micro-phase separation is increased concurrently with the length of soft-segment block. However, competition between enthalpic and entropic factors in the study of PUET10 and PUES20 samples led to different results by various methods. Ester-based TPUs showed higher Young's modulus and lower elongation-at-break compared to ether-based counterparts.

References

1. Akindoyo JO, Beg MDH, Ghazali S, Islam MR, Jeyaratnam N, Yuvaraj AR (2016) Polyurethane types, synthesis and applications—a review. RSC Adv 6:114453–114482
2. Ge C, Wang S, Zheng W, Zhai W (2017) Preparation of microcellular thermoplastic polyurethane (TPU) foam and its tensile property. Polym Eng Sci 58:E158–E166
3. Sahebi Jouibari I, Haddadi-Asl V, Mirhosseini MM (2019) Effect of nanofiller content and confined crystallization on the microphase separation kinetics of polyurethane nanocomposites. Polym Compos 40:E422–E430
4. Kopczyńska P, Datta J (2016) Rheological characteristics of oligomeric semiproducts gained via chemical degradation of polyurethane foam using crude glycerin in the presence of different catalysts. Polym Eng Sci 57:891–900
5. Pedrazzoli D, Manas-Zloczower I (2016) Understanding phase separation and morphology in thermoplastic polyurethanes nanocomposites. Polymer 90:256–263
6. Yilgör I, Yilgör E, Wilkes GL (2015) Critical parameters in designing segmented polyurethanes and their effect on morphology and properties: a comprehensive review. Polymer 58:A1–A36
7. Choi T, Weksler J, Padsalgikar A, Runt J (2009) Influence of soft segment composition on phase-separated microstructure of polydimethylsiloxane-based segmented polyurethane copolymers. Polymer 50:2320–2327
8. Velankar S, Cooper SL (1998) Microphase separation and rheological properties of polyurethane melts. 1. Effect of block length. Biomacromol 31:9181–9192
9. Petrović ZS, Javni I (1989) The effect of soft-segment length and concentration on phase separation in segmented polyurethanes. J Polym Sci Part B Polym Phys 27:545–560
10. Sinturel C, Bates FS, Hillmyer MA (2015) High χ-low N block polymers: how far can we go? ACS Macro Lett 4:1044–1050
11. Leung LM, Koberstein JT (1986) DSC annealing study of microphase separation and multiple endothermic behavior in polyether-based polyurethane block copolymers. Macromolecules 19:706–713
12. Sahebi Jouibari I, Haddadi-Asl V, Mirhosseini MM (2018) Formulation of micro-phase separation kinetics of polyurethane nanocomposites. Polym Adv Technol 29:2909–2916
13. Khordad R, Mirhosseini MM, Mirhosseini B (2017) Electronic, mechanical and thermodynamic properties of ceramic compounds. Iran J Sci Technol Trans Sci 1:1–9
14. Mirhosseini MM, Haddadi-Asl V, Zargarian SS (2016) Fabrication and characterization of polymer-ceramic nanocomposites containing pluronic F127 immobilized on hydroxyapatite nanoparticles. RSC Adv 6:80564–80575
15. Li S, Fried J, Colebrook J (2013) Molecular simulations of poly(2,5-benzimidazole): effect of water concentration, phosphoric acid doping, and temperature on hydrogen bonding and vehicular diffusion. Polym Eng Sci 53:597–608
16. Rahmati M, Modarress H, Gooya R (2012) Molecular simulation study of polyurethane membranes. Polymer 53:1939–1950
17. Tao HJ, Fan CF, MacKnight WJ, Hsu SL (1994) Application of a molecular simulation technique for prediction of phase-separated structures of semirigid model polyurethanes. Macromolecules 27:1720–1728
18. Madkour TM, Azzam RA (2013) Non-Gaussian behavior of self-assembled thermoplastic polyurethane elastomers synthesized using two-step polymerization and investigated using constant-strain stress relaxation and molecular modeling techniques. Eur Polym J 49:439–451
19. Wang X, Xu J, Li L, Liu Y, Li Y, Dong Q (2016) Influences of fluorine on microphase separation in fluorinated polyurethanes. Polymer 98:311–319
20. Avaz S, Oguz O, Kurt H, Menceloglu YZ, Atilgan C (2017) Soft segment length controls morphology of poly(ethylene oxide) based segmented poly(urethane-urea) copolymers in a binary solvent. Comput Mater Sci 138:58–69
21. Zhang C, Hu J, Ji F, Fan Y, Liu Y (2012) A combined experimental and computational study on the material properties of shape memory polyurethane. J Mol Model 18:1263–1271
22. Chen KS, Yu TL, Chen YS, Lin TL, Liu YJ (2001) Soft-and hard-segment phase segregation of polyester-based polyurethane. J Polym Res 8:99–109
23. Burattini S, Greenland BW, Merino DH, Weng W, Seppala J, Colquhoun HM, Hayes W, Mackay ME, Hamley LW, Rowan SJ (2010) A healable supramolecular polymer blend based on aromatic π–π stacking and hydrogen-bonding interactions. J Am Chem Soc 132:12051–12058
24. Mirhosseini MM, Rahmati M, Zargarian SS, Khordad R (2017) Molecular dynamics simulation of functionalized graphene surface for high efficient loading of doxorubicin. J Mol Struct 1141:441–450
25. Pangon A, Dillon GP, Runt J (2014) Influence of mixed soft segments on microphase separation of polyurea elastomers. Polymer 55:1837–1844
26. Król P (2007) Synthesis methods, chemical structures and phase structures of linear polyurethanes. properties and applications of linear polyurethanes in polyurethane elastomers, copolymers and ionomers. Prog Mater Sci 52:915–1015
27. Knychała P, Timachova K, Banaszak M, Balsara NP (2017) 50th anniversary perspective: phase behavior of polymer solutions and blends. Macromolecules 50:3051–3065
28. Chen X, Yuan C, Wong CKY, Zhang G (2012) Molecular modeling of temperature dependence of solubility parameters for amorphous polymers. J Mol Model 18:2333–2341
29. Lodge TP, Muthukumar M (1996) Physical chemistry of polymers: entropy, interactions, and dynamics. J Phys Chem 100:13275–13292
30. Velankar S, Cooper SL (2000) Microphase separation and rheological properties of polyurethane melts. 2. Effect of block incompatibility on the microstructure. Macromolecules 33:382–394
31. Chen TK, Chui JY, Shieh TS (1997) Glass transition behaviors of a polyurethane hard segment based on 4,4′-diisocyanatodiphenylmethane and 1,4-butanediol and the calculation of microdomain composition. Macromolecules 30:5068–5074
32. Vilensky AV, Lipatov Y (1994) A criterion for microphase separation in segmented polyurethane and polyurethane ureas. Polymer 35:3069–3074
33. Mirhosseini MM, Haddadi-Asl V, Zargarian SS (2016) Fabrication and characterization of hydrophilic poly (ε-caprolactone)/pluronic P123 electrospun fibers. J Appl Polym Sci 133:43345
34. Ruzette AVG, Mayes AM (2001) A simple free energy model for weakly interacting polymer blends. Macromolecules 34:1894–1907

35. Shahrousvand M, Mir Mohammad Sadeghi G, Shahrousvand E, Ghollasi M, Salimi A (2017) Superficial physicochemical properties of polyurethane biomaterials as osteogenic regulators in human mesenchymal stem cells fates. Colloids Surf B Biointerfaces 156:292–304
36. Shahrousvand M, Mir Mohammad Sadeghi G, Salimi A (2016) Artificial extracellular matrix for biomedical applications: biocompatible and biodegradable poly(tetramethylene ether) glycol/poly(ε-caprolactone diol)-based polyurethanes. J Biomater Sci Polym 27:1712–1728
37. Shahrousvand E, Shahrousvand M, Ghollasi M, Seyedjafari E, Sahebi Jouibari I, Babaei A, Salimi A (2017) Preparation and evaluation of polyurethane/cellulose nanowhisker bimodal foam nanocomposites for osteogenic differentiation of hMSCs. Carbohydr Polym 171:281–291